Mechanistic and Computational Study of Cinnabar Phase Transformation: Aplications and Implications to Preservation of this Pigment in Historical Painting | 2005-02

Arizona State University

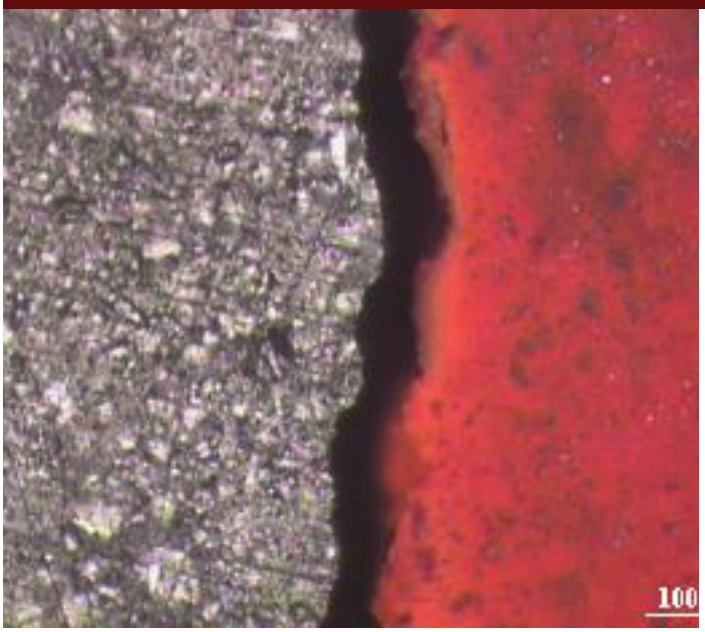

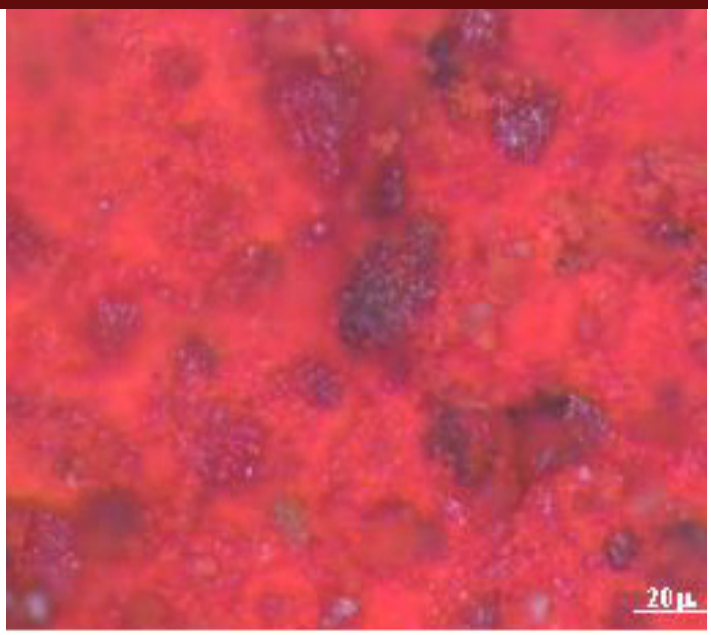

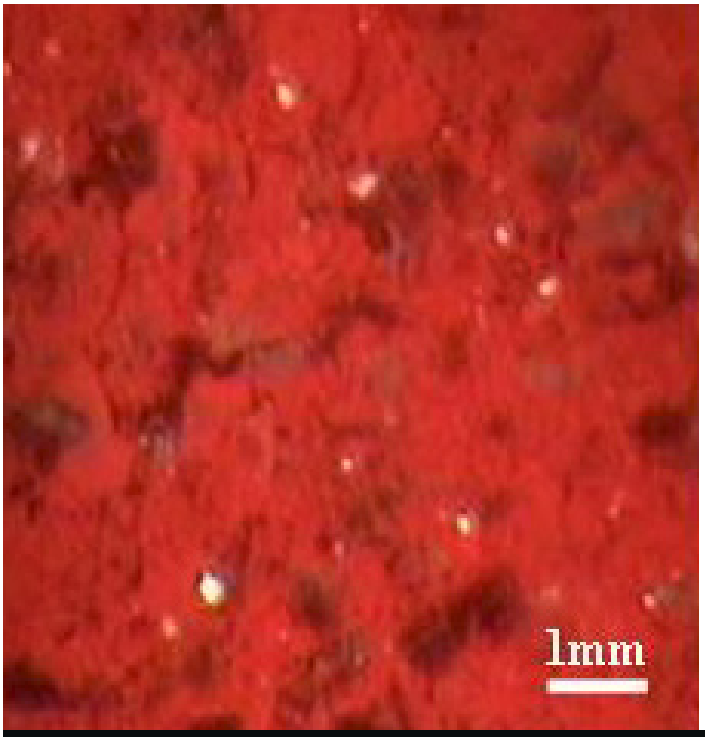

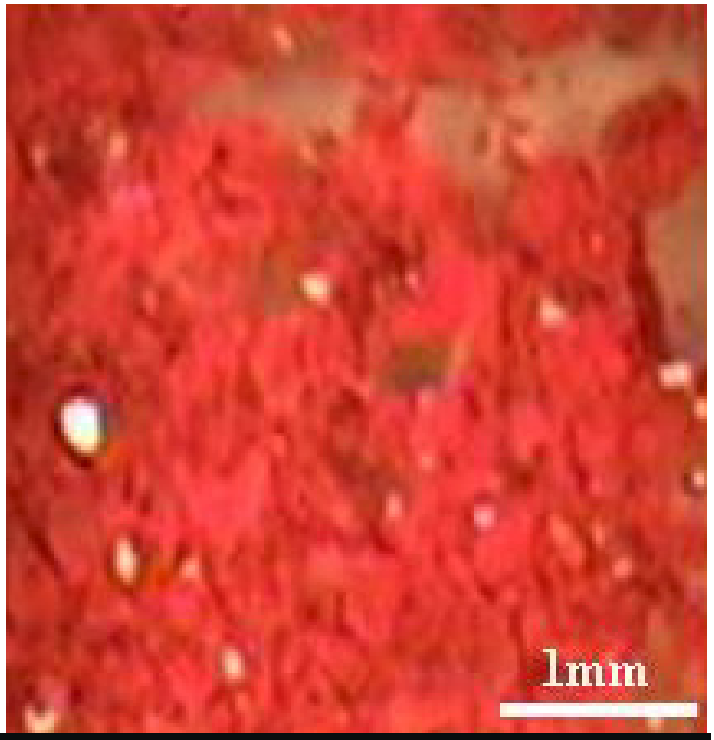

National Park Service
U.S. Department of the Interior

National Center for Preservation Technology and Training

MECHANISTIC AND COMPUTATIONAL STUDY OF CINNABAR PHASE TRANSFORMATION: APPLICATIONS AND IMPLICATIONS TO THE PRESERVATION OF THIS PIGMENT IN HISTORICAL PAINTING

Hamdallah Béarat[1,*], Andrew Chizmeshya[1], Renu Sharma[1], Alix Barbet[2], Michel Fuchs[3]

[1] *Center for Solid State Science, Arizona State University, Tempe, AZ 85287-1704, USA;*
[2] *CEPMR, CNRS, Ecole Normale Supériore, 75005 Paris, France;*
[3] *Institut d'Archéologie et des Sciences de l'Antiquité, Université de Lausanne, Lausane, Switzerland*

ABSTRACT

Blackening of cinnabar (α-HgS) constituted a dilemma for ancient artists and modern conservators as well. In this research program, the mechanisms of HgS phase transformation were studied using several analytical techniques: scanning electron microscopy, energy dispersive spectroscopy, X-ray powder diffraction, Raman spectroscopy, and cathodoluminescence spectroscopy. The experimental study was coupled with advanced computational modeling of materials using *Ab initio* density functional theory methods. Natural and synthetic standards representing both hexagonal (α-HgS) and cubic (β-HgS) polymorphs of mercuric sulfide were submitted to several kinds of physical treatment to induce transformation in either direction and the products were characterized using appropriate analytical method.

Experimental work shows that physical parameters such as radiation, mechanical activation or thermal treatment can induce the transformation in one or the other direction. The results obtained to date, suggest that blackening is due to amorphization and formation of an intermediate phase, thus following a "nucleation and growth" mechanism. Meanwhile, modeling of the structure shows that the polymorphic difference is primarily associated with the expansion of the *c*-axis in going from cinnabar to metacinnabar. It also indicates that optical behavior of these two phases is inherently related to the structure of their respective band gaps. The combination of the two approaches has thus proved very powerful in understanding the mechanism of the phase transformation, which is central to any successful preservation of the red pigment and to the restoration of its color once blackened.

* Corresponding Author Information: Center for Solid State Science, Arizona State University, P. O. Box 871704, Tempe, AZ 85287-1704, USA. Phone: +1 (480) 965-2624, Fax #: +1 (480) 965-9004, E-mail Address: hamdallah.bearat@asu.edu.
Supported by the National Center for Preservation Technology and Training, National Park Service, U.S. Department of the Interior, under Grant No. MT-2210-02-NC-12

INTRODUCTION

Cinnabar (α-HgS) or vermilion is a curious material. The word *cinnabar* came from the Latin *cinnabaris* derived from the Greek *kinnabari*, which itself is a Hindu word meaning dragon's blood. The pigment was named **cinnabar** by the Greeks but *minium* by the Romans [1-3]. Minium now refers only to red lead (Pb_3O_4). Cinnabar or vermilion was very appreciated by the Ancients (in China, Greece and Roman Empire). The Chinese already knew how to prepare the pigment artificially from the native elements as early as 2nd Millennium B.C [4]. In the Roman period, it is reported that the mine in Spain was submitted to the control of the government [2]. The extraction of the mineral was limited at 2000 lbs per annum, which was delivered under seal directly to Rome. The refinement of the ore locally was forbidden and it was entrusted to a company at Rome. Its price was 50 sesterces a pound and a law fixed its maximum price at 70 sesterces a pound. The pigment was adulterated with red lead by the company [2].

Several uses are known for cinnabar. The most common use was as a red pigment for painting [5-12]. It could also have been used to prepare metallic mercury by thermal decomposition [2-3]. Cinnabar had also some limited use in religious ceremonies [2-3], in funerary as preservative [13], or in cosmetics [14]. In classical times, it was also used as a red pigment for the preparation of ink in Ancient China [4] and the Middle East [15]. Cinnabar continued to be widely used as pigment for both illumination and painting through the medieval and renaissance periods [11,16-17]. However, modern applications for cinnabar include its use as photoelectric and semiconductor materials [18]. Both forms of mercury sulfide (α-HgS or cinnabar and β-HgS or metacinnabar) are being considered as structural models for a new generation of semiconductors (II-VI) [19-22].

The detection of cinnabar in an ancient painting is long regarded by archaeologists and art historians as indicator of the owner's economic and social "standing" and may also indicate the rank of the skillful artist [7]. It usually attests of the high quality and sophistication of the painting (in terms of materials, technique, and style) [5-9]. It was also suggested that its use in a given civilization might have some chronological significance [7]. In any case, there is evidence of a more elaborated painting technique for its use in the Roman period [5-6,8-9]. Whenever it had to be used, a special care was given to the preparation and application of the paint and of its support. It is worth noting that in most cases, cinnabar was applied on a special type of plaster composed of lime and calcite crystals (or marble dust), whereas a plaster composed of lime and river sand was in common use for most pigments [5-6].

The main problem with cinnabar pigment is that it often blackens. Light was suspected as responsible for this color change. The Romans, for instance, knew this phenomenon and have developed a special and somewhat complicated technique to protect it from blackening [1-2]. However, investigation has shown that despite these precautions the pigment has blackened in several cases [6,9,23] (Figure 1). Meanwhile, blackening of cinnabar may sometimes be associated with fire in the place [24,25] or to exposure to

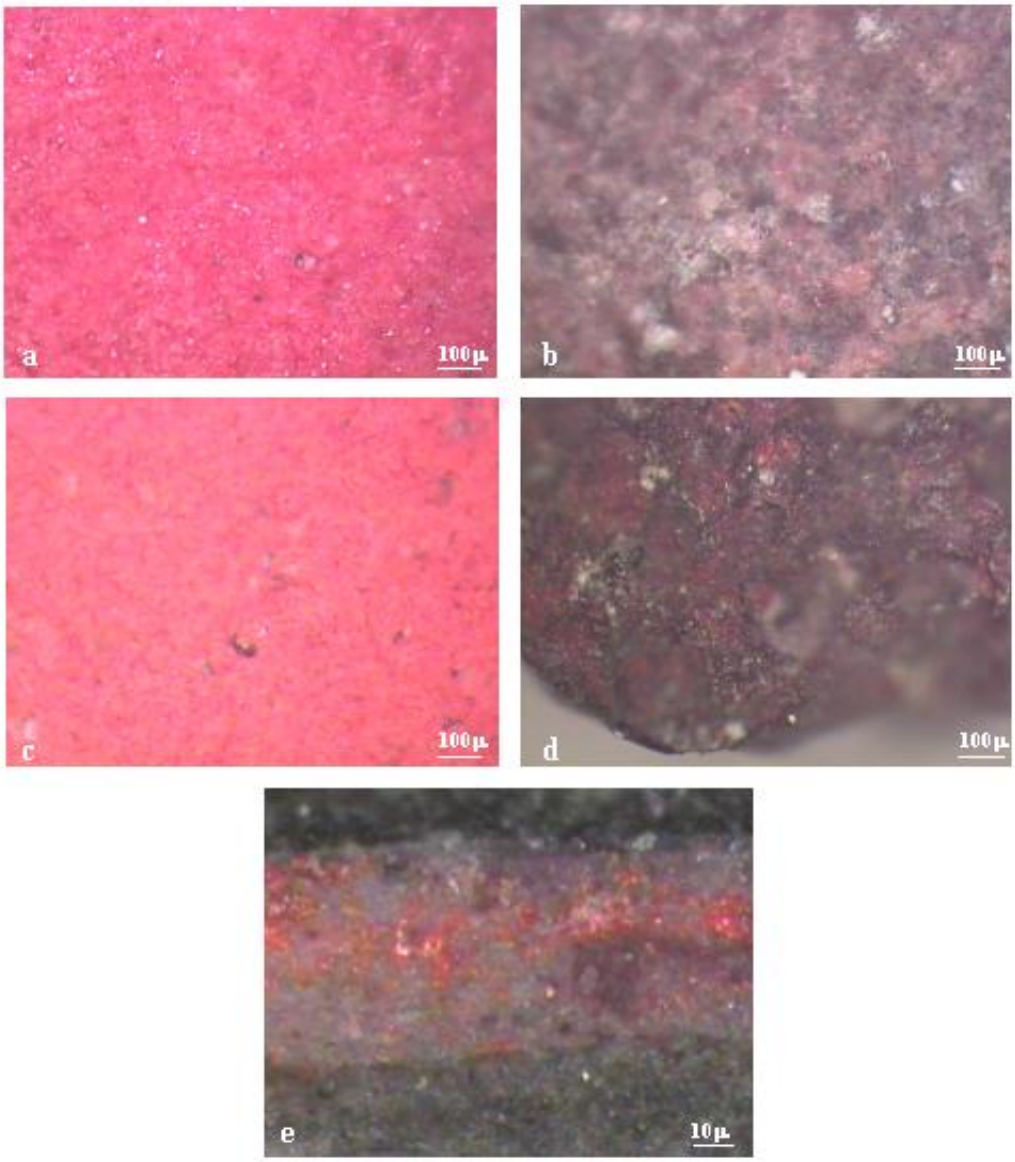

Figure 1 Some archaeological samples of cinnabar: (a) and (b) Gallo-Roman wall painting fragments from Reims, France (2nd Century A.D.); (c) and (d) pigments from the pyramid of the Hieroglyphic Stairway at the Classic Maya site of Copán, Honduras (400-600 A.D.) after and before grinding; (e) a cross section of a Gallo-Roman wall painting from Insula 7, Avenches, Switzerland (2nd Century A.D.).

sunlight and to open air [23]. Indeed, some laboratory studies have shown the red pigment to darken upon exposure to light [26,27]. The presence of alkali salts and some organic compounds may accelerate the transformation of cinnabar [27]. Laser cleaning of painting containing cinnabar may also cause darkening of the vermilion paint [28].

Blackening of cinnabar (α-HgS, which has a hexagonal structure) is thought to originate from its transformation into metacinnabar (β-HgS, which is black and has a cubic structure). Surprisingly, metacinnabar has never been detected in blackened paints. However, a dark grayish amorphous phase is also known to exist. It is also known that α-HgS is more stable at lower temperatures and it can only transform to β-HgS at a temperature in excess of 380ºC [18]. The meta-stable phase structure can be retained even after cooling. Impurities can cause α-HgS to convert to β-HgS at lower temperatures [21]. Indeed, the few published data on this transformation do not allow a satisfactory understanding of the mechanism of this reaction and the different factors that govern the forward or backward reaction. This understanding is vital to design of a process that can help protecting this color in painting and enables the restoration of the original color when darkening occurs. We present in this paper the major results of a mechanistic and computational study of the phase transformation of mercury sulfide (HgS) and its implications to the conservation of the red pigment in historical paintings.

MATERIAL AND METHODS

Description of materials used

Table 1 below shows the list of samples of cinnabar and metacinnabar acquired and used in the experimental work. Cinnabar samples consisted of three types of materials: natural single crystals from Ukraine, natural polycrystalline from Spain, and synthetic powder from Alfa Aesar Co. Metacinnabr material consisted of several natural polycrystalline samples from CA, USA as well as synthetic powder from Alfa Aesar Co.

Several sets of archaeological samples were acquired for the second phase of the study and therefore submitted to preliminary examination only. The first set consists of 21 fragments of wall painting fragments from different Gallo-Roman sites in France. Most are in very good state of conservation with no signs of blackening (Figure 1a), but some have blackened in some areas (Figure 1b). The second set comes from the pyramid of the Hieroglyphic Stairway at the Classic Maya site of Copán, Honduras (400-600 A.D.) and consists of several samples of blackened cinnabar raw pigment. Most of these samples exhibit a black or grayish exterior layer masking the red color of the pigment (Figure 1d). The third set consists of several wall painting fragments from the Gallo-Roman site of Avenches (*Aventicum*) in Switzerland. Figure 1e shows a cross section of one of these samples, which also has a thin black layer covering the painting.

Table 1: List of raw samples studied with their origin, phase composition, and structural data obtained by XRD and cell refinement.

Sample	**Origine**	**Description**	**System**	**Cell Parameters**
Cinnabar 1 α-HgS	Synthetic	Pure red powder	Sys: Hexagonal S.G.: $P3_221$	*a =4.147* *c=9.492*
Cinnabar 2 α-HgS	Nikitovka Mine Dombass, Ukraine	Pure red single crystals	Sys: Hexagonal S.G.: $P3_221$	*a =4.149* *c=9.501*
Cinnabar 3 α-HgS	Al-Maden Mine, Spain	Polycrystalline ground under acetone; pure red	Sys: Hexagonal S.G.: $P3_221$	*a =4.152* *c=9.502*
Cinnabar 3 α-HgS	Al-Maden Mine, Spain	Polycrystalline ground in air; dark brown	Sys: Hexagonal S.G.: $P3_221$	*a =4.152* *c=9.513*
Metacinnabar 1 β-HgS	Synthetic	Black powder (contains some cinnabar)	Sys: Cubic S.G.: $F\bar{4}3m$	*a=5.853*
Metacinnabar 2 β-HgS	Mt. Diablo Mine, CA, USA	Black polycrystalline	Sys: Cubic S.G.: $F\bar{4}3m$	*a=5.854*

Analytical Methods

A battery of methods was used to study such complicated problem. We summarize below the specifics of major methods employed:

X-Ray Diffraction (XRD):

This method was used to characterize the raw materials, to determine any phase changes occurring during any experiment, and to obtain structural information on each of the phases under consideration. Powder diffraction (XRD) patterns were obtained using a Rigaku D/MAX-IIB X-ray diffractometer with Cu$K\alpha$ radiation. Samples were ground, adhered to a glass slide by spraying a solution of petroleum gel in n-hexane in N_2 flow on the slide and then spreading the powder uniformly onto it. Scans were done for $2\theta = 2^o$ to 65^o and with steps of $0.01^o/s$.

Scanning Electron Microscopy/Energy Dispersive Spectroscopy:
For morphological changes selective samples were imaged using a Hitachi 4700 field-emission scanning electron microscope (FESEM). When required, elemental analysis of specific samples was accomplished via energy dispersive X-ray spectroscopy (EDS) using a EDAX Phoenix system coupled with the Hitachi 4700.

Raman Spectroscopy:
Raman spectra were obtained for single crystal materials as well as powders pressed into pellets using a green laser of 540 nm. To avoid excessive damage to the samples, the laser power was reduced to 10%.

Cathodoluminescence Spectroscopy:
Samples were analyzed in cathodoluminescence using a 5kV accelerating voltage, a beam current of 500pA, a slit of 1 mm, a 1000x magnification, a scan of range 200-800nm with a step size of 5, and at Room temperature.

RESULTS AND DISCUSSION

Characterization of natural and synthetic cinnabar and metacinnabar materials:

In a first stage, the research has focused on cinnabar and metacinnabar raw materials. The description of these samples, their place of origin, phase purity, and respective crystallographic data are given in Table 1. While all three cinnabar samples were found by X-ray diffraction (XRD) (Figure 2) to be phase pure, both metacinnabar samples were found to contain some cinnabar phase impurity. Refinement of the structure gave cell parameters in perfect agreement with theoretical ones. Cinnabar (α-HgS) crystallizes in the hexagonal system, with space group $P3_221$, and has the cell parameters of a=4.149Å and c=9.495Å. Metacinnabar (β-HgS) is cubic, space group $F\bar{4}3m$, and has a=5.853Å [29]. However, it seems that pure (metacinnabar) is hard to find or to prepare and its occurrence as single crystal is extremely rare. To overcome this difficulty, characterization of the β-phase was carried out using micro-analytical techniques such as micro-Raman, cathodoluminescence (CL), and FE-SEM and we also intend to separate small crystals of this phase under the microscope and assure their purity for bulk-based analyses.

Further characterization of the natural samples was performed using micro-Raman and cathodoluminescence spectroscopy. Micro-Raman spectroscopic analysis was performed to characterize the two HgS phases. Figure 3 gives the cinnabar spectrum with three characteristic bands at 250 cm^{-1}, 285 cm^{-1}, and 348cm^{-1}. The bands on this spectrum are within 4 cm^{-1} from the published values for this phase [30,31]. Figure 4 shows the Raman spectrum obtained for the natural polycrystalline metacinnabar. It exhibits a sharp band at 171 cm^{-1} and two week and broad ones at 285 cm^{-1} and 950 cm^{-1}, respectively. No published Raman spectra for this phase could be found, and therefore further analysis is needed before this spectrum be confirmed.

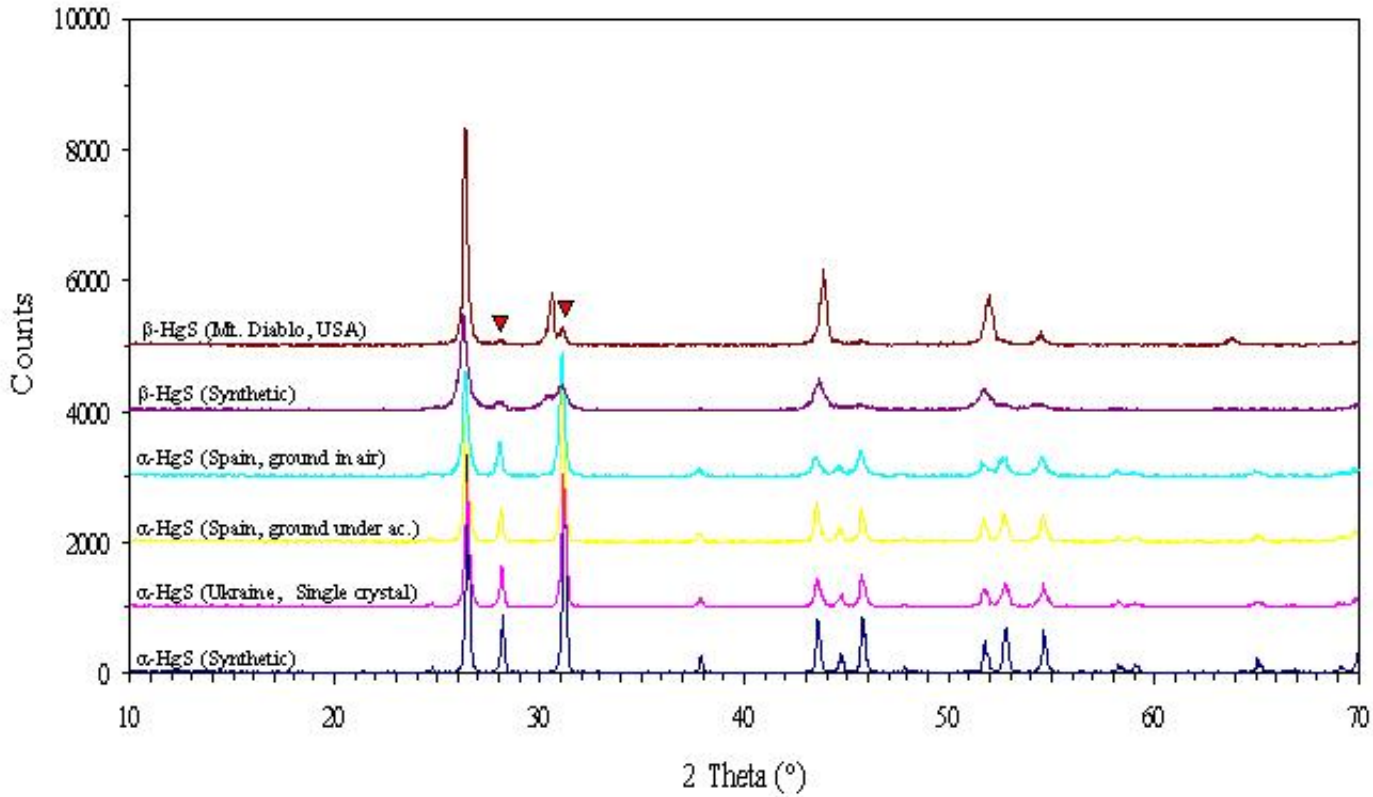

Figure 2 X-ray powder diffraction patterns for the the raw samples. While all cinnabar (α-HgS) samples are phase pure, both synthetic and natural metacinnabar (β- HgS) contain some cinnabar as phase impurity (reflections indicated with red triangles) .

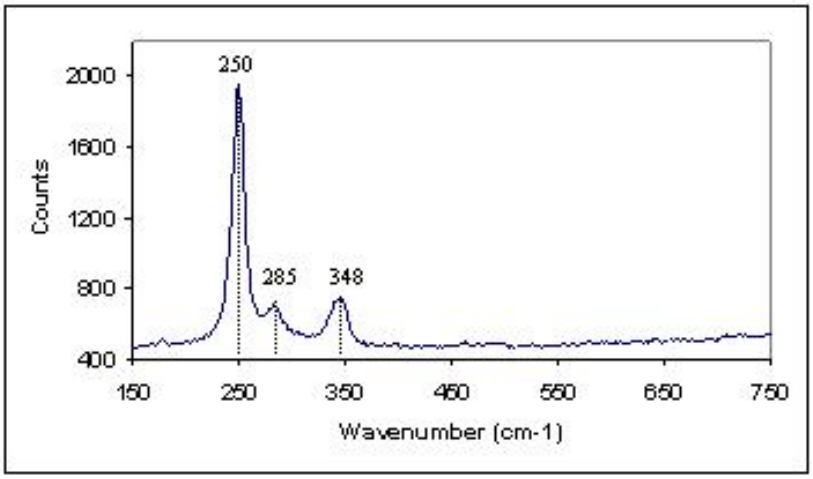

Figure 3 Raman spectrum obtained for cinnabar (α-HgS) single crystal from Ukrania using a green laser of λ=540 nm.

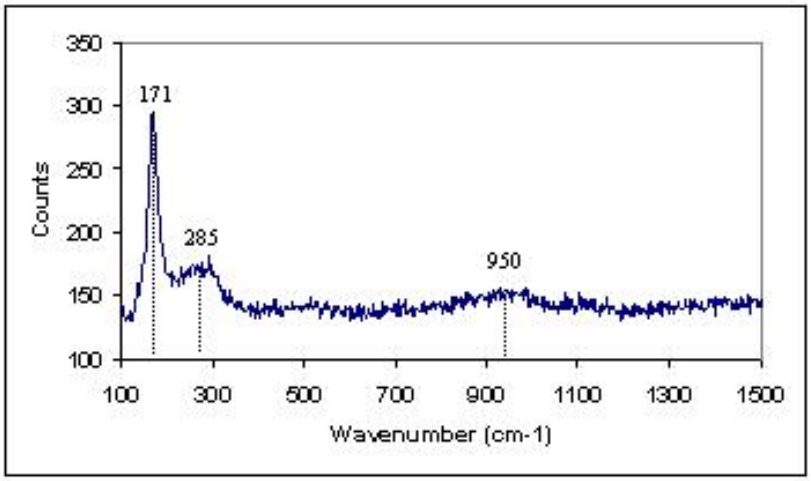

Figure 4 Raman spectrum obtained for metacinnabar (β-HgS) polycrystalline material from Mont Diablo, CA, USA using a green laser of λ=540 nm.

These two samples also were analyzed with cathodoluminescence spectroscopy and their spectra are given in Figure 5 below. Cinnabar has a unique luminescence component in the red with a maximum at 585nm. This wavelength is equivalent to 2.1 eV, characteristic band gap for cinnabar (see modeling section below). Metacinnabar, however, does not show any luminescence, which is consistent with its black color and its low band gap (~1.6eV).

Transformation of cinnabar to metacinnabar and vice versa:

Stability of cinnabar:

Two types of experiments have shown cinnabar to be unstable. In the first, blackening occurred upon grinding the pigment in air and a brownish color was obtained (Figure 6 a & d). In the contrary, grinding of cinnabar under acetone did not cause any change of color (Figure 6c). For the blackened sample, the red color was recovered by moderate heating in air at 100°C (Figure 6 b & e). Analysis of the sample shown in Figure 6d with XRD shows grinding has two effects on cinnabar crystal structure (light blue pattern in Figure 2). On one hand there is broadening of cinnabar reflection lines, indicating some amorphization of the structure. On the other hand, some of the reflections are slightly shifted towards higher *d*-spacing (lower angles). Refinement of the structure shows a slight increase in the *c*-parameter for this sample (Table 1). This result is consistent with modeling calculations that predict an increase in the *c*-parameter as α-HgS transforms into β-HgS (see modeling section below). Raman spectroscopic analysis of this sample (Figure 7a) only shows bands attributable to cinnabar. Cathodoluminescence analysis of the same sample shows two luminescence components at 350nm (in the UV) and 625nm (in the red-orange), respectively. These luminescence components come from two distinct parts of the sample (see images under the curve). Further work is certainly needed before a satisfactory explanation of this change is reached.

Another type of experiment related to the stability of cinnabar, is the effect of radiation. At this level, two observations have been made. The first concerns the effect of exposure to a laser during Raman analysis. High power radiation and longer periods of exposure lead to decomposition of cinnabar. The two laser-induced spots shown in Figure 8a below have holes at their centers surrounded by a network of channels (Figure 8 b & c). A quite similar effect was observed for the exposure to electrons. In both cases, decomposition of cinnabar and volatilization of both mercury and sulfur occurs, as attested by the formation of the deep holes and channels. However, blackening also occur at least at the very beginning of exposure. Table 2 below shows the chemical composition and Hg:S ratios at the exposure spot as compared to a fresh surface. It seems that the transformation is initiated by loss of sulfur, leaving the structure deficient in this element and thus confirming the prediction of calculations on the change in the band gap towards the black. Another observation that confirms the decomposition effect of the laser is shown in Figure 7a. As the exposure time increases, the intensity of the characteristic bands of cinnabar diminishes in intensity under the effect of the laser, while characteristic bands of

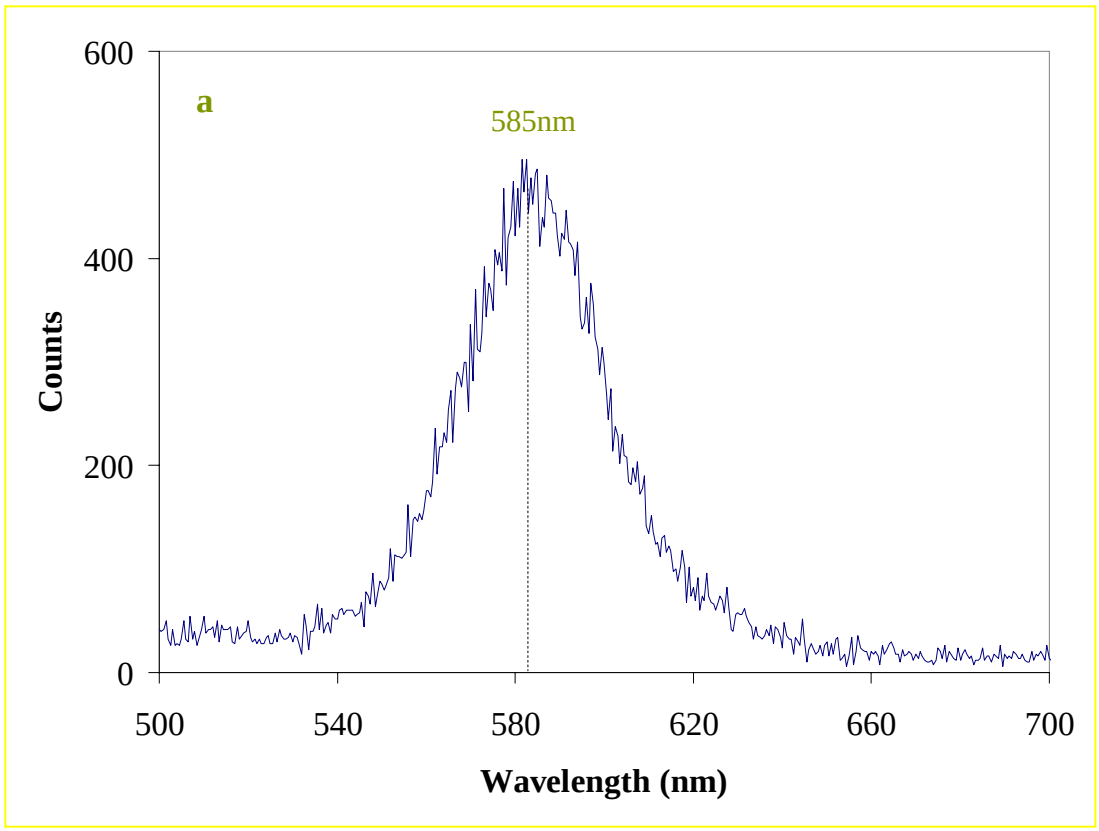

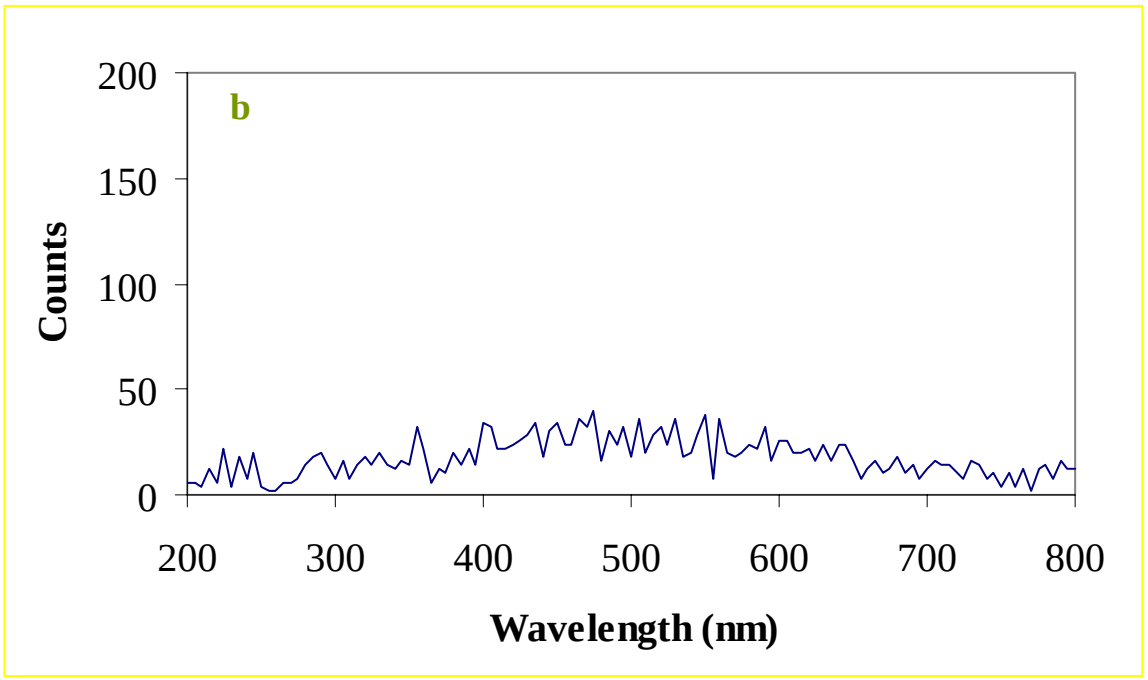

Figure 5: Cathodoluminescence spectra of (a) single crystal cinnabar from Ukraine and (b) polycrystalline metacinnabar from Mt. Diablo, CA, USA.

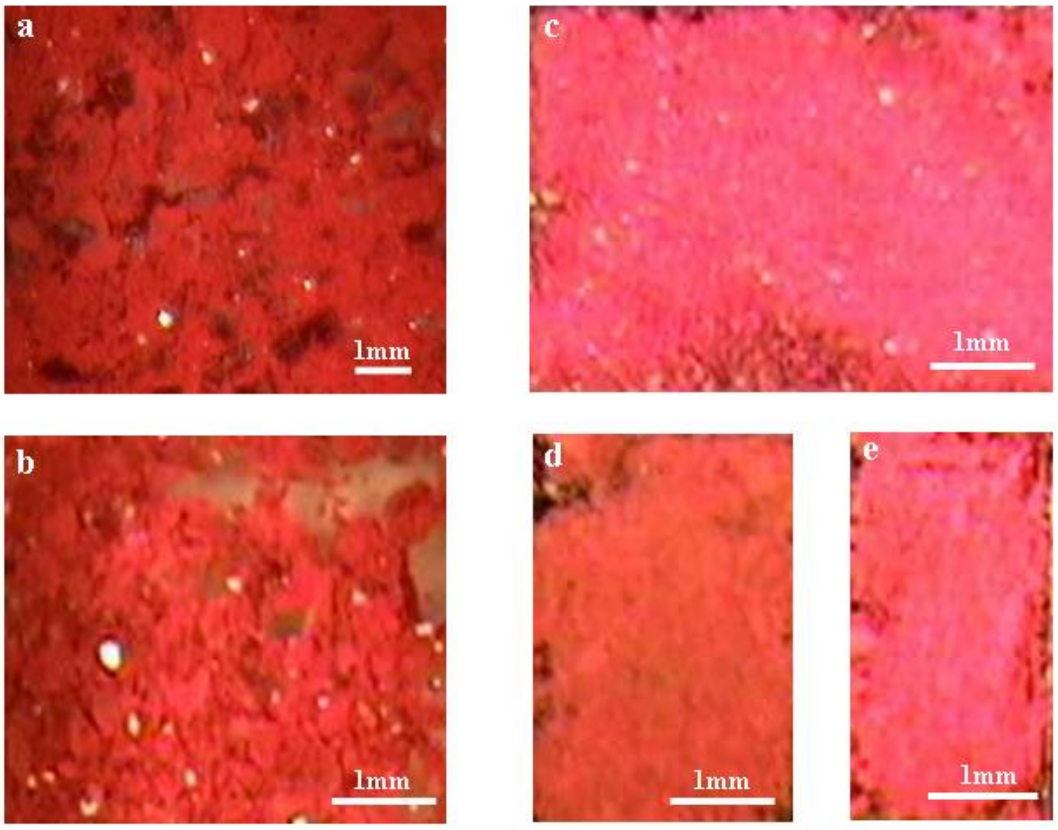

Figure 6: (a) Single crystal cinnabar from Ukraine ground in air and (b) same sample after heat treatment at 100°C in air. Polycrystalline cinnabar from Spain, (c) ground under acetone, (d) ground in air, and (e) same sample in (d) after heat treatment at 100°C in air.

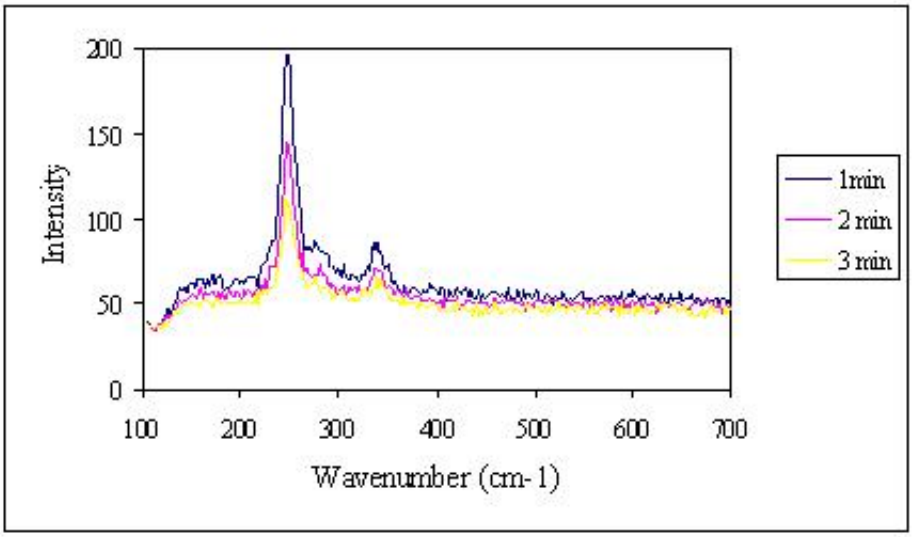

(a)

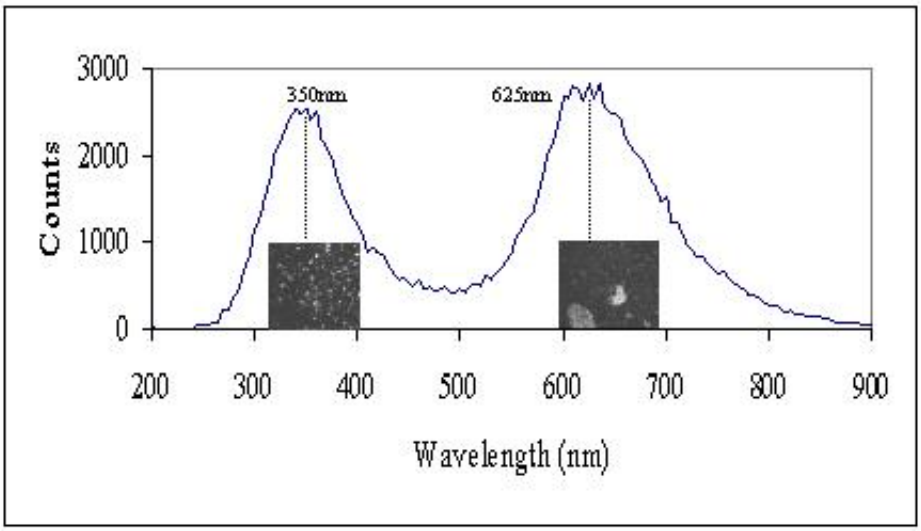

(b)

Figure 7 (a) Micro-Raman spectra of blackened cinnabar obtained by grinding cinnabar from Spain in air after 1, 2, and 3 minutes of exposure to the laser; (b) cathodoluminescence spectrum of the same sample with CL images of the zones emitting in the UV (350nm) and in the red-orange (625nm).

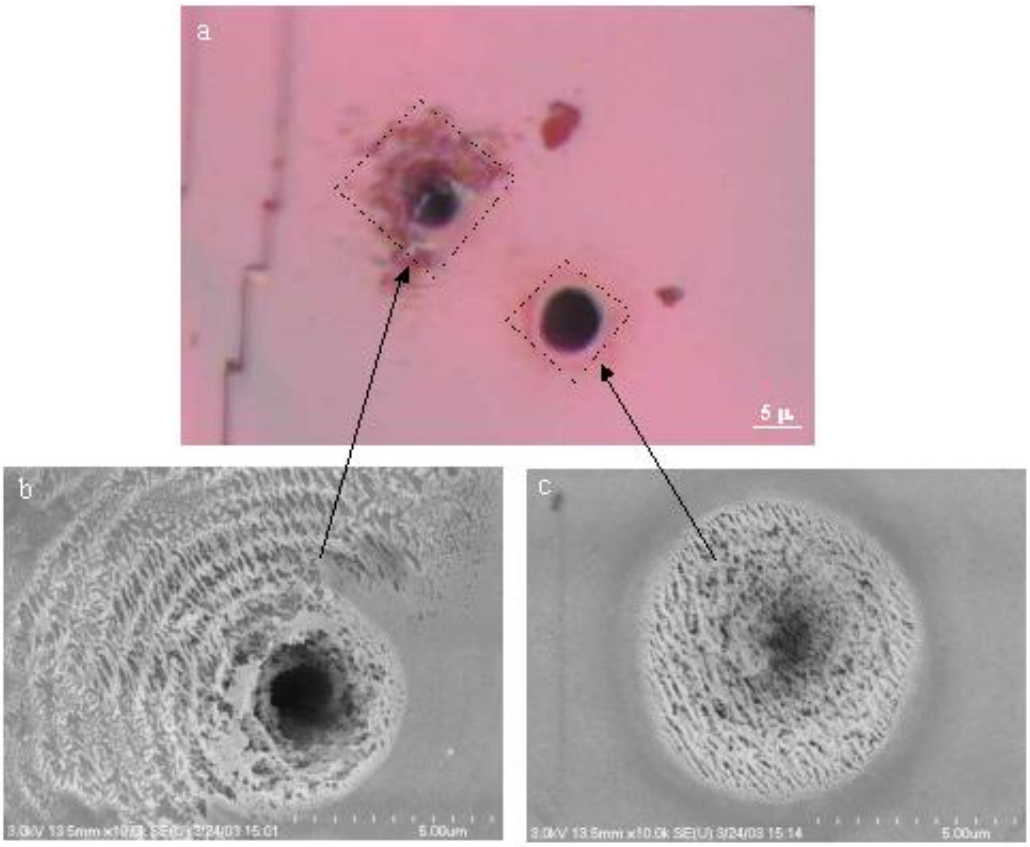

Figure 8 (a) A single crystal cinnabar from Ukraine analyzed with micro-Raman spectroscopy showing two laser-induced black spots; (b) and (c) black spots shown in (a) imaged with FE-SEM.

Table 2: Chemical composition (expressed in atomic %) of a black spot caused by irradiation with electrons (15kV, 10μA) as compared to that of a fresh zone.

	Fresh Zone	**Irradiated Zone**
Hg (Atomic %)	45.80	50.83
S (Atomic %)	54.20	49.17
Hg/S Ratio	0.85	1.03
% Sulfur Deficiency	0	18.26

metacinnabar do not appear, suggesting that laser-induced alteration is decomposition and not phase transformation.

Stability of metacinnabar:

The preliminary experiments performed on blackened cinnabar (Figure 6) and synthetic metacinnabar (Figure 9) shows that backward transformation to cinnabar is quite possible using controlled heat-treatment. Blackening effect can be overcome by moderate heating in air at low temperature (100°C) for a few minutes, whereas transformation of metacinnabar into cinnabar requires higher temperatures (>300°C) and longer period of time (hours).

Structural and Electronic modeling of Mercuric sulfide (HgS)

Simulation studies using first principles quantum mechanical modeling methods were undertaken to elucidate the structure-composition relationship in HgS, which is implicated in the blackening mechanism [32-34]. It is therefore of great interest to clearly establish the connection between the atomic level structure of various HgS polymorphs and their corresponding electronic and optical behavior. In the first phase of this project our primary modeling goal has been to validate efficient predictive modeling methods based on density functional theory. This is achieved by performing benchmark calculations on the cinnabar and metacinnabar phases of mercuric sulfide, and comparing the known corresponding experimental properties.

Ab initio density functional theory methods have already been applied to a wide range of electronically related systems sharing similar structural polymorphism including ZnSe, ZnTe, CdSe, and CdTe [35], but calculations have apparently not been reported for mercuric sulfide. Heavy elements are currently within the reach of modern all-electron

simulation techniques such as the full potential linearized augmented plane wave (FPLAPW) method. Important core electron relativistic effects, which influence the optical properties of, e.g., the color of metallic gold *via* core-valence coupling, can now be reliably and routinely calculated. Although we have this capability, it is computationally elaborate and expensive. For this reason, our exploratory results are based on the projected augmented wave (PAW) variant [36] of the plane wave pseudopotential (PWPP) method as implemented within the VASP electronic structure simulation code [37].

Computational Strategy

All calculations were performed using density functional theory within the local density approximation (LDA) for exchange-correlation effects, as implemented within the VASP code [37]. It is well known that the LDA underestimates bond lengths in solids and molecules by ~ 1-2% and overestimates binding energy. For this reason we also used the generalized gradient approximation (GGA) which substantially improves the energetic description in solids and molecules, but leads to a slight overestimate in bond lengths. We employed ultra-soft pseudopotentials and a plane wave basis to generate the ground state structures and electronic states of all HgS phases considered. The standard computational parameters (e.g., plane wave energy cutoff, and density of k-points) were converged to ensure that the theoretical limit was attained in all cases. Typically a plane-wave cutoff of E_{cut} ~ 600 eV, and a 6x6x3 Monkhorst-Pack *k*-point grid density was found to be sufficient. With these parameters we obtain reasonable agreement with the experimental structural parameters, as shown in Table 3 which compares the LDA and GGA structural parameters for the cinnabar and metacinnabar phases of HgS.

Preliminary Results: Discussion

The structural results, listed in Table 3, were obtained by minimizing the quantum mechanical forces on all of the atoms in the cinnabar and metacinnabar crystallographic cells. The cinnabar structure is found to be the ground state structure in the static lattice limit (thermal effects are neglected in our preliminary treatment). In order to facilitate the comparison between the cinnabar and metacinnabar structures, the latter phase case recast in to a hexagonal setting from its usual zincblende cubic form. This is achieved by defining the c-axis in a tripled cell setting along the conventional cubic [111] direction. In this way, the equivalent hexagonal cell has $a_H=a/\sqrt{2}$ and $c_H=\sqrt{3}a$, where "a" is the conventional cubic cell parameter (see Figure 10). Our results show a marked difference between the LDA and GGA results. Typically, the LDA/GGA lead to an under/over-estimate of the lattice parameters, but here we see that the GGA matches the experimental values in cinnabar while the LDA exhibits the expected underestimate. It must be emphasized that an underestimate of several % is anticipated in a static lattice approximation. Thermal expansion would lead to an increase in all crystalline length scales. Thus, LDA gives the most plausible and realistic trends for both phases and we proceed with our analysis of the associated electronic structure on this basis. Note that within the common crystalline

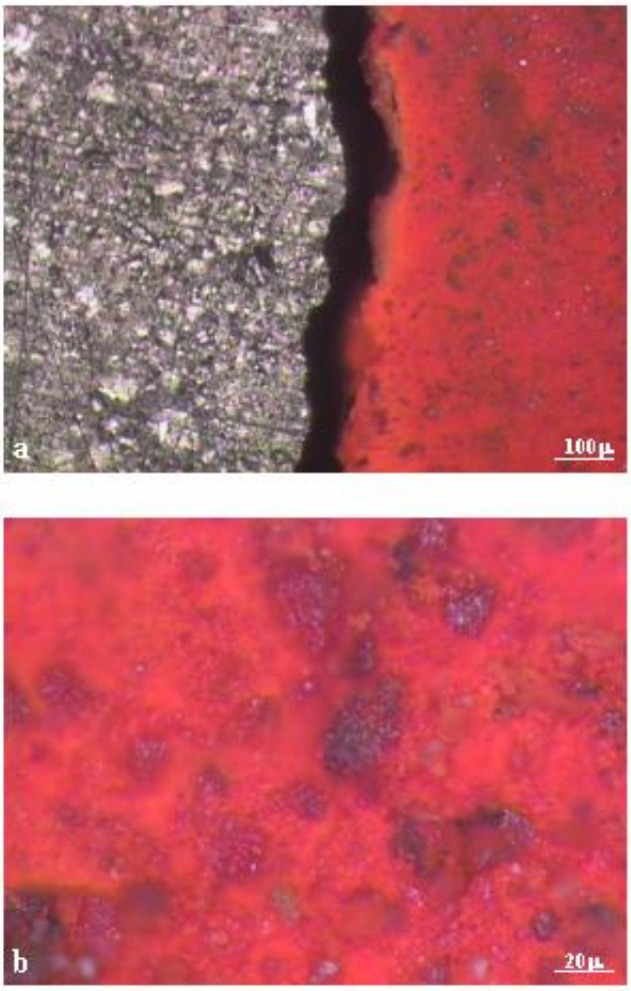

Figure 9 (a) Synthetic metacinnabar powder pressed into a pellet and its half on right was heat-treated at 335°C in air. (b) higher magnification of the red on the right showing pseudomorphic growth of cinnabar after metacinnabar.

Table 3: *Ab initio* simulation results for the structures of cinnabar (α-HgS**)** and metacinnabar (β-HgS) obtained using the VASP code. The metacinnabar structure is given here in terms of a tripled cell (3C setting) of the conventional zincblende cubic structure (a=5.852 Å). The equivalent hexagonal cell has $a_H=a/\sqrt{2}$ and $c_H=\sqrt{3}a$. The experimental figures are emboldened.

α-HgS ($P3_221$)						
	a(Å)	b(Å)	c(Å)	α	β	γ
LDA	4.027	4.027	9.333	90	90	120
GGA	4.145	4.145	9.496	90	90	120
EXP	**4.149**	**4.149**	**9.495**	**90**	**90**	**120**

β-HgS ($F\bar{4}3m$ **)**						
	a(Å)	b(Å)	c(Å)	α	β	γ
LDA	4.119	4.119	10.067	90	90	120
GGA	4.241	4.241	10.371	90	90	120
EXP	**4.139**	**4.139**	**10.138**	**90**	**90**	**120**

setting established in our case, the metacinnabar basal plane parameters are almost identical, and that the polymorphic difference is associated primarily with the expansion of the c-axis in going from cinnabar to metacinnabar.

The electronic band structure was computed based on the converged equilibrium LDA ground state atomic structure and charge density. The LDA typically underestimates the band gap in semiconducting materials. We obtained improved estimates by correcting the band gaps using a generalized density function theory (GDFT) approach developed by Fritsche and co-workers [38,39]. The correction amounts to a ~ 0.91 eV shift between the cinnabar valence and conduction band states, leading to a predicted gap of ~ 2.1eV in good agreement with experiment, while a similar treatment of the metacinnabar band structure leads to a gap of about ~0.9 eV. This is somewhat less than that obtained experimentally and may be due to the presence of a strained structure of metacinnabar. The intrinsic errors in using this approach are reduced from ~ 100% to about 15% for cinnabar. The band

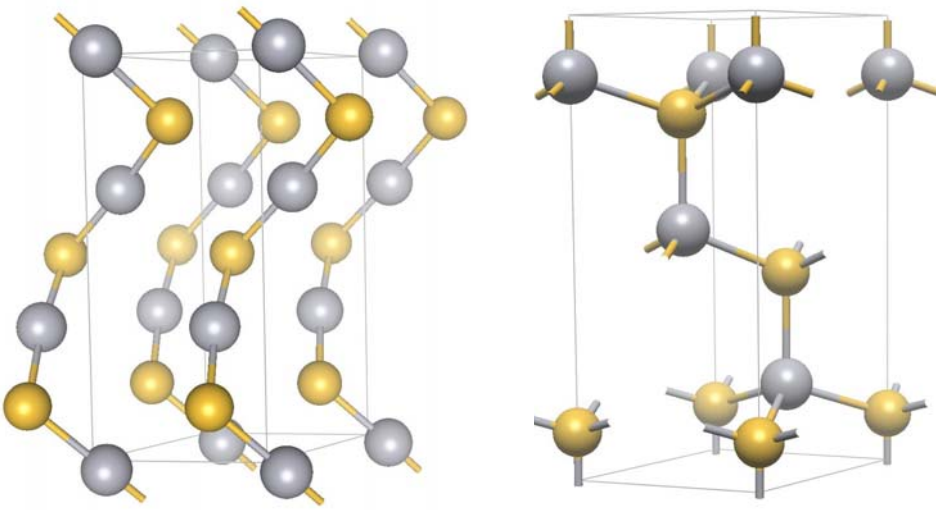

Figure 10: Structural models of the cinnabar (left panel) and metacinnabar (right panel) phases of HgS. The metacinnabar structure is given here in terms of a tripled cell (3C setting) of the conventional zincblende cubic structure (a=5.852 Å). The equivalent hexagonal cell has $a_H = a/\sqrt{2}$ and $c_H = \sqrt{3}a$.

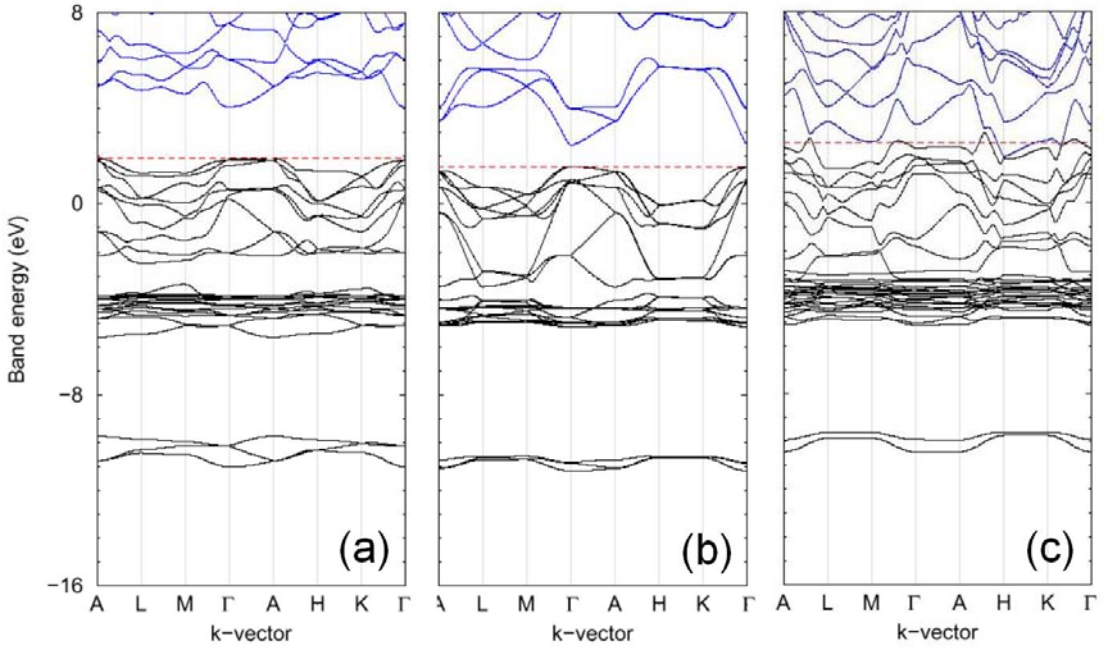

Figure 11: GGA band structure for: (a) Cinnabar, (b) meta-cinnabar and (c) an isostructural mercuric sub-sulfide ($Hg_{0.66}S_{0.33}$) showing the significant change in the band-gap responsible for structure of cinnabar and metacinnabar are shown in Figure 11 (a) and (b), respectively. A full analysis of the origin of the various bands will be developed through the course of the the observed color change due to structural polymorphism (cubic metacinnabar in the 3C, Z=3 cell). Valence bands, black; conduction bands, blue; Fermi level, red dashed.

project work. This will aid in the interpretation of the experimental results, including the origin of color change and its relationship to the atomic/crystalline structure.

We have also begun to explore the effect of altering the ratio of Hg to S within the lattice. In order to explore small stoichiometric changes a large supercell containing ~ 50 atoms would be needed. For now, a bounding estimate can be obtained by simply substituting one of the sulfur atoms by mercury. Within the setting of the cells shown in Figure 10, the replacement of a sulfur atom by mercury leads to the composition $Hg_{0.66}S_{0.33}$. The ground state crystalline structure is found to be a slightly distorted monoclinic version of the cinnabar phase with a 0.8% dilation of the basal *a*-parameter and a ~ 2.4 % increase in the *c*-axis length. The corresponding band structure is shown in Figure 11(c) which indicates that extreme sulfur deficiency results in the closure of the band gap and a metallic or semi-metallic behavior. These structural and electronic trends are understandable, and a more elaborate and detailed analysis should be planned for the future.

Implications to conservation of cinnabar in painting

Computational study indicates that color change in cinnabar may occur through chemical change (particularly, loss of sulfur) or physical change through reconfiguration and expansion of the lattice. These effects may well correspond to beam damage effects (radiolysis or inelastic scattering and the *knock-on* damage [40]) commonly encountered in electron microscopy and Raman studies. Both effects have been observed in the case of cinnabar and supported by the experimental work: sulfur deficiency by EDX analysis (Table 2) and XRD shows a slight shift in the *d*-spacing of some blackened cinnabar reflections toward higher values (the (012) plane for example as in Figure 15 below). However, experimental work also indicates that blackening of cinnabar may also occur through amorphization that may be induced by grinding in air[§] or by interaction with sunlight.

To simulate some practical conditions of the use of cinnabar pigment in historical paintings, a different set of experiment was conducted with synthetic cinnabar. It aimed at verifying the effect of direct sunlight and the role the painting media in favoring or inhibiting the blackening. Six different media were tested: water, $Ca(OH)_2$, beeswax, linseed oil, tempera, and petroleum gel in n-hexane. The pigment was dispersed in each medium and then spread on 3 identical glass slides, labeled with the particular medium. The slides were then place on a flat surface and covered with Pyrex glass beakers. The samples were exposed to the direct Arizona sunlight and monitored regularly for any change for 8 months. The tested media show substantial difference in their protective power. They range from water being the least protective to $Ca(OH)_2$, beeswax, petroleum gel, tempera, and linseed oil being the most protective (Figure 12). Blackening is already

[§] It is probably worth reminding here that Pliny in his Natural History mentions that in his time cinnabar was being ground under water.

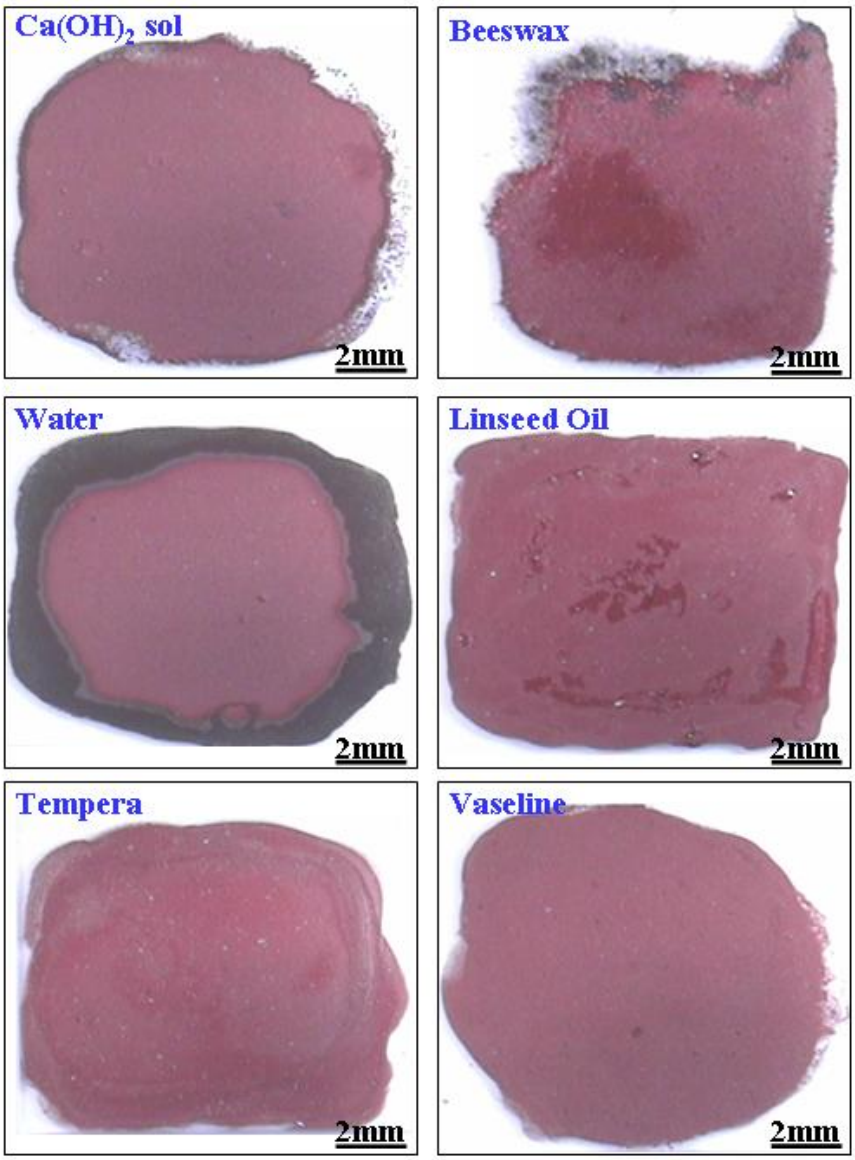

Figure 12: Combined effect of painting media and sunlight on color of cinnabar pigment. The paint films shown here were prepared with different media, brushed onto glass slides and exposed to direct Arizona sunlight. The images shown in the figure here were taken after 8 months of exposure.

visible with water after a month and it started at the edge of the preparation and progressed inward. With $Ca(OH)_2$ change was similar but much slower. In the case of beeswax, change was much faster at one end of the preparation and was accompanied with loss of material, probably by volatilization. In all other three media the change is negligible, but the pigment is shiner with linseed oil. These observations were confirmed on all three samples prepared with each medium.

To better understand the mechanism of the blackening, a blackened water-prepared paint sample was chosen for further analysis. It was studied with FE-SEM and with XRD. The blackened zone at the edge and the central red zone were analyzed separately with XRD. The remaining part of the preparation was then studied with FE-SEM. Pigment grains were imaged from the edge and inward. As Figure 13 shows, a remarkable difference in grain morphologies is seen as one move from the edge inward. Obviously, the blackening is associated with amorphization of cinnabar. At the edge of the paint preparation, the grains are converted to some spongy amorphous agglomerates. In the central part however, despite very slight change, the grains still show their crystal facets. The change is therefore slow, but progressive (Figure 14). Since it starts at the edge and progresses inward, this suggests that it follows a "nucleation and growth" mechanism. This may probably explain why the change starts at the edge, where the grains are more exposed to environmental agents than those at the center.

XRD analysis of the above mentioned preparation shows a general broadening of the reflections of the black area with respect to those of the red area. Broadening of XRD lines is usually attributed to amorphization of the material. But, XRD analysis also shows that for the black area some reflections are being shifted toward higher *d*-spacing. This is most obvious for the (012) reflection, as shown in Figure 15. Indeed, the center of the peak is shifted by 0.004Å left side from its position at 2.875 Å, which corresponds to about 10% of the full-peak width. It is worth noting that *d*-spacing of the most discriminant reflection of metacinnabar is located at 2.923 Å. Although formation of metacinnabar could not be so far confirmed as plausible final product of blackening, one cannot exclude its presence in the form of very small crystallites that may look amorphous in XRD. Therefore, the most plausible description of the blackening of cinnabar is as a continuous process of amorphization.

Preliminary examination of some ancient pigments with important signs of blackening has confirmed the previous statements. Most of these samples exhibit a black or grayish exterior layer masking the red color of the pigment (Figure 1d), but after grinding the red color is recovered (Figure 1c). Similarly, XRD analysis only shows cinnabar reflections. This indicates that in this case blackening only concerns a very thin layer, which probably acts as a protective layer for cinnabar from further transformation. Figure 1e shows a cross section of a Roman painting sample, which also has a thin black layer covering the painting. In this image, one also notices a dark zone at the interface painting/plaster, while the core of the paint layer is still conserved. These observations should direct conservation efforts aiming at protecting and/or restoring the cinnabar color of these samples.

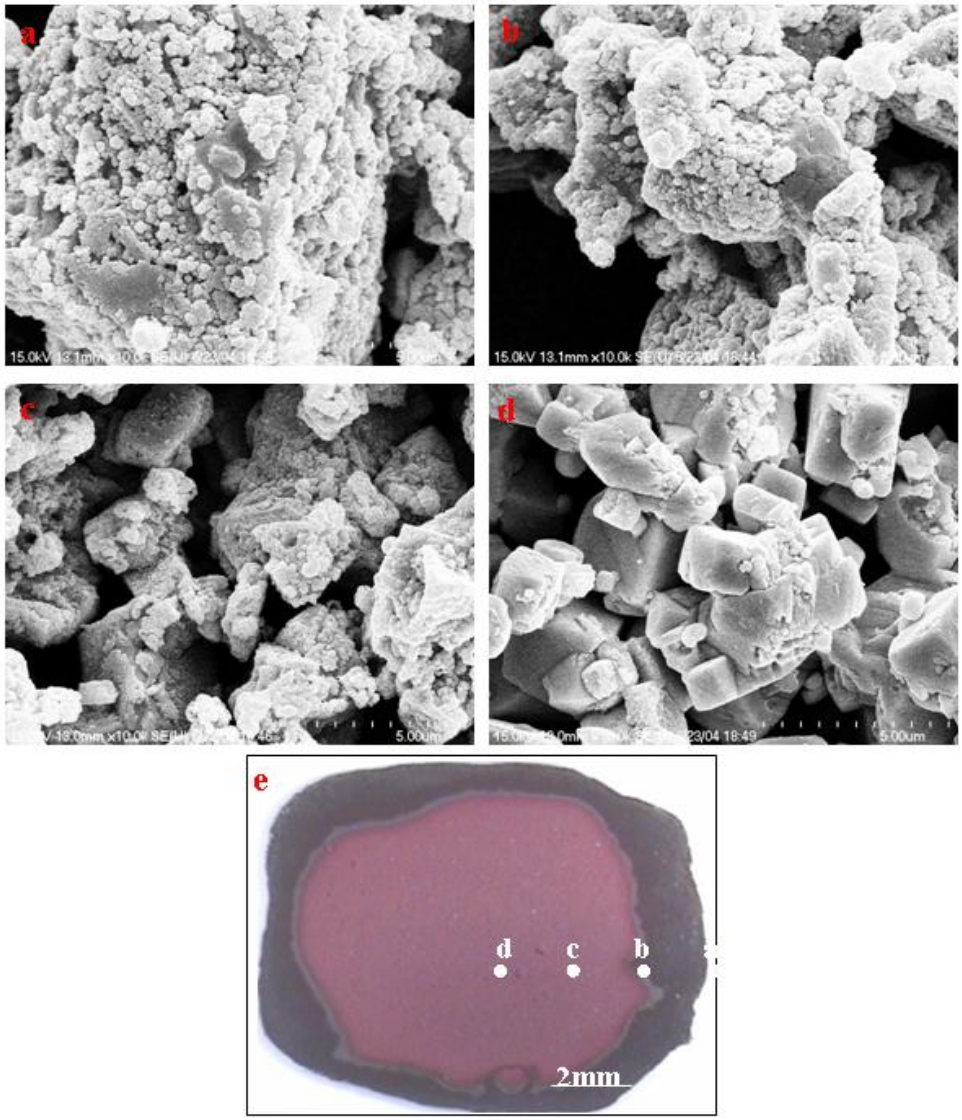

Figure 13: Secondary electron images of points *a* through *d* shown on the optical micrograph *e* obtained with Field Emission Gun Scanning Electron Microscopy. The paint was prepared by mixing cinnabar with water and spread on a glass slide that was exposed to direct sunlight for 8 months. Note the amorphization of the pigment (cinnabar) in the black zone at the edge of the paint preparation. Imaging conditions are: 15kV accelerating voltage, 10mA beam current, 13mm working distance, and 10k magnification.

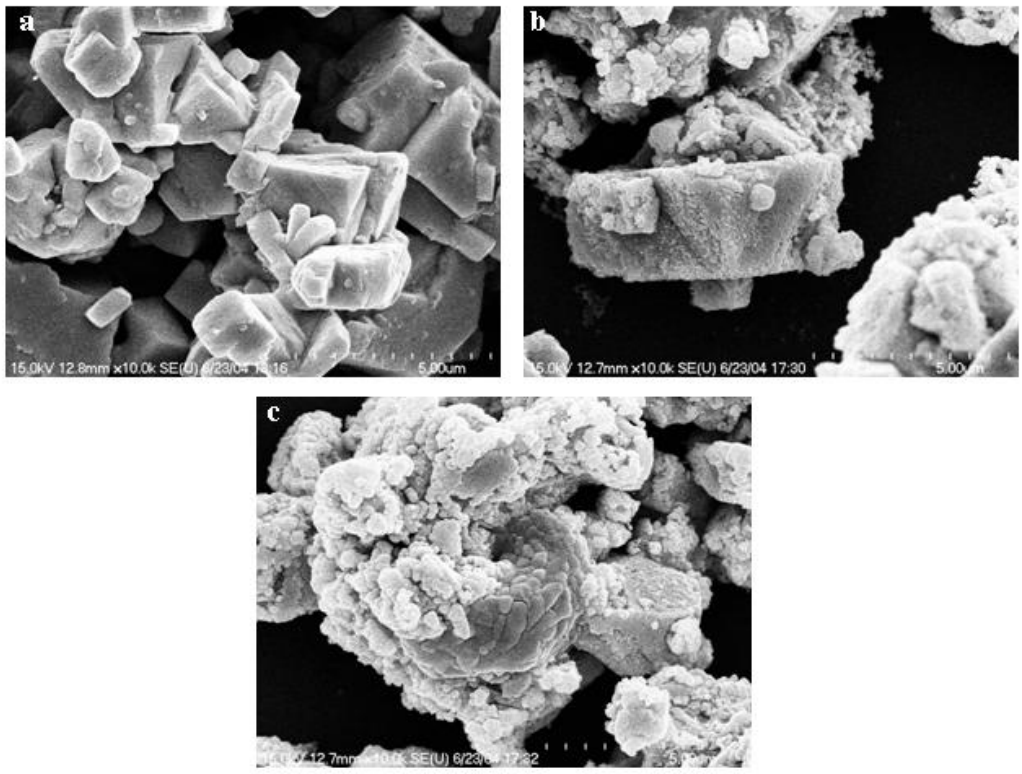

Figure 14: FE-SEM micrographs taken for different areas in cinnabar paint prepared with H_2O as medium after 8 months of exposure to direct sunlight: (a) crystals slightly affected; (b) moderately affected where the black product still maintain the parent crystal form; (c) heavily amorphized pigment where the product shows a spongy porous texture.

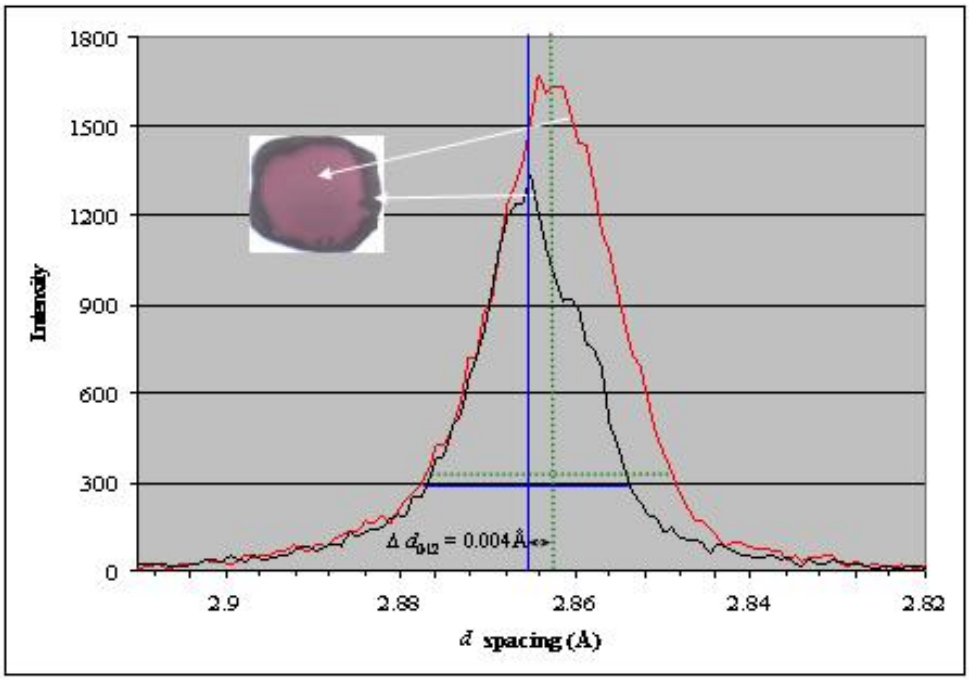

Figure 15: Shift of the (012) d-spacing, as measured by X-ray diffraction, of the blackened zone relative to the red zone of vermilion paint preparation after exposure to direct sunlight for 8 months.

Conclusions and projection for future research

Since only the first phase of this research project has received funding, and hoping that further support will soon be available to complete the second phase, we would like to hint future research in this area. In the first place, efforts should focus on determining the different factors that favor transformation of cinnabar into metacinnabar or vice versa. In addition to the factors already surveyed such as mechanical activation (grinding), heat-treatment, irradiation, and effect of medium, eventually some other factors such as impurities (Fe, Zn, Cd) in cinnabar, presence of soluble salts, direct contact of HgS with water and other environmental agents such as O_2, H_2O, H_2S, etc., as well as eventual use of restoration/preservation products should be examined as well. The attempt to study *in situ* the phase transformations of HgS with high resolution electron microscopy unfortunately did not provide satisfactory insight into the mechanisms of HgS phase transformations, since both materials have proved to be very sensitive to radiation damage. An alternative would be to use the environmental cell scanning electron microscope instead. In fact, ASU has acquired an E-SEM and is functional only recently. This microscope is equipped with a heating-cooling stage and a controlled-atmosphere chamber that will allow dynamic observation of the transformation of cinnabar into metacinnabar and vice versa. Once further funding becomes available, we intend to take full advantage of this facility to better understand the mechanisms that govern this phase transformation. Our ultimate goal would be to have full control of the transformation in both directions to better tackle the restoration of precious historical samples.

The simulation work should equally go hand in hand with the experimental efforts throughout the research, with an emphasis on elucidating the relationship between the optical and structure behavior of various HgS polymorphs. The treatment of the phase stability of cinnabar, metacinnabar, and eventually their intermediate amorphous phase, must be expanded to include the effects of temperature and mechanical stresses. Also, the effect of the atmosphere (oxidizing or reducing) on the stability of HgS needs to be explored, by calculating the structural and electronic (optical) implications of systems such as HgO_xS_{1-x} where x is small. As both Hg and S are vulnerable to beam damage and proved to highly volatile, as the TEM experiments have shown, some exploratory lattice dynamics studies can therefore be done to examine the relative diffusivities of Hg and S at the surface of cinnabar. Although the topic of desorption and degassing is very challenging and computationally daunting, simulation should provide some crude estimates which may provide important insight into the interpretation of experimental studies.

To conclude for this first phase of research project on blackening of cinnabar, the experimental work has provided three important findings:

(1) Natural blackening of cinnabar is a continuous process of amorphization that starts at the crystal surface in contact with the surroundings rather than congruent transformation to metacinnabar, as widely speculated. This change can be induced by direct sunlight as well as by mechanical stress.

(2) The black intermediate amorphous phase may act as a protective layer for cinnabar from further change. The amorohization/blackening process can be reversed simply by moderate heating to about 100°C with no significant loss of material. However, heating at higher temperatures may cause decomposition/volatilization of cinnabar and consequently significant loss of material.

(3) The laser and electron-induced change in cinnabar is a destructive process. It follows a different mechanism, radiolysis and knock-on damage that leads to important material loss. This effect should be taken with extreme care when cleaning and or conserving cinnabar pigment in painting.

Acknowledgment

We are grateful to the National Center for Preservation Technology and Training, National Park Service, US department of the Interior for funding this project. We thank the Center for Solid State Science for use of the Goldwater Materials Science Laboratories, including the Materials Facility, and the High Resolution Electron Microscopy Facility. We thank the Department of Chemistry and Biochemistry for the use of the X-ray Diffraction Facility and the Raman Spectroscopy Facility. We also wish to thank Professor George Wolf for the micro- Raman analysis; Professor Fernando Ponce from the Department of Physics and Sridhar Serivisan from the Science & Engineering PhD Program for CL analysis, and Professor Ray Carpenter from the Center for Solid State Science for the valuable and helpful discussions. We also thank the Center for Solid State Electronic Research for the use of the FE-SEM facility.

References

[1] Vitruvius, *The Ten Books of Architecture*. French Translation, Perrault C. (Ed.), Errance, Paris (1986).

[2] Pliny The Elder, *Natural History*, XXXIII. French Translation, Zehnacker H. (Ed.), Les Belles Lettres, Paris (1983).

[3] Pliny The Elder, *Natural History*, XXXV. French Translation, Croiselle J. M. (Ed), Les Belles Lettres, Paris (1985).

[4] R. J. Gettens, G. L. Stout, 1966, *Painting materials: a short encyclopaedia*, New York (2nd Ed.) 170-173.

[5] H. Béarat, 1996, Chemical and mineralogical analyses of Gallo-Roman wall painting from Dietikon, Switzerland, *Archaeometry*, **38** [1] 81-95.

[6] H. Béarat, M. Fuchs, 1996, Analyses physico-chimiques et minéralogiques de peintures murales romaines d'Aventicum, I: du pigment à Avenches, *Bulletin Pro Aventico* **38**, 35-49.

[7] A. Barbet, 1990, L'emploi des couleurs dans la peinture murale romaine antique, in: *Pigments et Colorants de l'Antiquité et du Moyen Age*, Colloque International du CNRS, Paris, 255-270.

[8] M. Fuchs, E. Ramjoué, 1994, *Commugny: splendeurs murales d'une villa romaine*, Catalogue d'exposition, Nyon.
[9] M, Fuchs, H. Béarat, 1997, Analyses physico-chimiques et peintures murales romaines à Avenches, Bösingen, Dietikon et Vallon. In: *Roman Wall Paintings: Materials, Techniques, Analysis and Conservation*. Proceedings of the International Workshop, Fribourg, 7-9 March 1996, H. Béarat, M. Fuchs, M. Maggetti, D. Paunier, (Eds.), 181-191.
[10] R. Cesareo, F. V. Frazzoli, C. Mancini, S. Sciuti, M. Marabelli, P. Mora, P. Rotondi, G. Urbani, 1972, Non-destructive analysis of chemical elements in paintings and enamels, *Archaeometry* **14** [1], 65-78.
[11] L. Burgio, D. A. Ciomartan, R. J. H. Clark, 1997, Pigment identification on medieval manuscripts, paintings and other artifacts by Raman microscopy: applications to the study of three German manuscripts, *Journal of Molecular Structure* **405**, 1-11.
[12] R. J. Gettens, R. L. Feller, W. I. Chase, 1972, Vermilion and Cinnabar, *Studies in Concervation* **17**, 45-69.
[13] J. Martin-Gil, F. J. Martin-Gil, G. Delibes-de-Castro, P. Zapatero-Magdaleno, F. J. Sarabia Herrero, 1995, The first known use of vermilion, *Experientia* **51**[8], 759-761.
[14] M. Yamada, T. Minami, G. Yamada, Y. Tohno, S. Tohno, Y. Ikeda, T. Tashiro, Y. Kohno, K. Kawakami, 1997, Different element ratios of red cosmetics excavated from ancient burials of Japan, *The Science of the Total Environment* **199**, 239-298.
[15] Y. Nir-El, M. Broshi, 1996, The red ink of the Dead Sea scrolls, *Archaeometry* **38** [1], 97-102.
[16] S. Bruni, F. Cariati, F. Casadio, L. Toniolo, 1999, Identification of pigments on a XV century illuminated parchment by Raman and FTIR microspectroscopies, *Spectrochimica Acta* **Part A 55**, 1371-1377.
[17] M. Bicchieri, M. Nardone, A. Sodo, 2000, Application of micro-Raman spectroscopy to the study of an illuminated medieval manuscript, *J. Cult. Heritage* **1**, S277-S279.
[18] J. Lamure, H. Brusset, 1962, Mercure. In: *Nouveau Traité de Chimie Minérale* **Tome V**, Pascal P., Ed., 733-797.
[19] J. Y. Raty, J. P. Gaspard, R. Céolin, R. Bellissent, 1997, A cinnabar local order in liquid II-VI compounds, *Physica* **B 234-236**, 364-366.
[20] A. San Miguel, A. Polian, J. P. Itié, 1995, A variable coordination structure in II-VI semiconductors: the cinnabar phase, *J. Phys.Chem. Solids* **56** [3/4], 555-558.
[21] W. Paszkowicz, W. Szuszkiewicz, E. Dynowska, J. Domagal, B. Witkowska, M. Marczak, P. Zinn, 1999, High-pressure-high-temperature study of $Hg_{1-x}Mn_xS$, *Journal of Alloys and Compounds* **286**, 208-212.
[22] J. Zeng, J. Yang, Y. Qian, 2001, A novel morphology controllable preparation method to HgS, *Materials Research bulletin* **36**, 343-348.
[23] A. Barbet, 1987, Qu'attendre des analyses de pigments, *PACT*, **17**, 155-169.
[24] H. Béarat, 1996, Les pigments à base de plomb en peinture murale romaine, in: *Preservation and restoration of Cultural Heritage: Stone Materials, Air Pollution, Murals-Scientific Research and Case Studies*, Proceedings of the 1995 LCP Congress, Montreux, R. Pancella (Ed.), Ecole Polytechnique Fédérale de Lausanne, 547-55.
[25] S. Rickerby, 1991, Heat alteration to pigments painted in the fresco technique, *The*

Conservator **15**, 39-44.
[26] R. L. Feller, 1967, Studies in the darkening of vermilion by light, *Reports and studies in the history of Art 1967*. National Gallery of Art, Washington D.C., 99-111.
[27] V. Daniels, 1987, The Blackening of Vermilion by Light, *Recent Advances in the Conservation and Analysis of Artifacts,* Summer Schools Press, London, 280-282.
[28] P. Pouli, D. C. Emmony, C. E., Madden, I., Sutherland, 2001, Analysis of the laser-induced reduction mechanisms of medieval pigments, *Applied Surface Science* **173**, 252-261.
[29] J. Lima-de-Faria, 1994, "Structural Mineralogy: An Introduction", Solid Earth Sciences Library, Vol. 7. Kluwer Academic Publishers, Dordrech.
[30] H. G. Edwards, D. W. Farwell, F. Rull Perez, J. Medina Garcia, 2001, Mediaeval cantorals in the Valladolid Biblioteca: FT-Raman spectroscopic study, *The Analyst*, **126** [3], 383-88.
[31] R. L. Frost, H. G. M. Edwards, L. Duong, J. T. Kloprogge, W. N. Martens, 2002, Raman Spectroscopic and SEM study of cinnabar from Herod's palace and its likely origin, *The Analyst*, **127** [2], 293-96.

[32] P. Pouli, D.C. Emmony, C.E. Madden, I. Sutherland, Analysis of the laser-induced reduction mechanisms of medieval pigments, *Appl. Surf. Sci.* **173** (2001) 252.
[33] R.J. Gettens, H. Kuhn, W.T. Chase, in: A. Roy (Ed.), *Artists Pigments*, Vol. 2, Oxford University Press, New York, 1993.
[34] M. Doerner, in: The Materials of the Artist (and Their Use in Painting), Revised Edition, Harcourt, Brace and Jovanovich, New York, 1984.
[35] Ab initio calculations of the pressure-induced structural phase transitions for four II-VI compounds, Michel Cote, Oleg Zakharov, Angel Rubio, and Marvin L. Cohen, *Phys.Rev.* B. **55**, 13025 (1997).
[36] P.E. Blochl, *Phys. Rev.* B **50** (1994) 17953.
[37] G. Kresse and J. Furthmuller, *Comput. Mater. Sci.* **6**,15 (1996); G. Kress and J. Hafner, *Phys. Rev. B* **4**7, 558 (1993); G. Kresse and J.J. Furthmuller *ibid.* **5**4,11 169 (1996).
[38] L. Fritsche and Y.M Gu, *Phys. Rev.* B **48**, 4250 (1993).
[39] L. Fritsche , *Phys. Rev.* B **33**, 3976 (1986); *Physica* B **172**, 7 (1991).
[40] D. B. Williams, C.B. Carter, *Transmission Electron Microscopy, I Basics.* Plenum Press New York (1996).